Large-scale motions and self-similar structures in compressible turbulent channel flows

Cheng Cheng [1] and Lin Fu [1,2,3,*]

[1]*Department of Mechanical and Aerospace Engineering, The Hong Kong University of Science and Technology, Clear Water Bay, Kowloon, Hong Kong*

[2]*Department of Mathematics, The Hong Kong University of Science and Technology, Clear Water Bay, Kowloon, Hong Kong*

[3]*HKUST Shenzhen-Hong Kong Collaborative Innovation Research Institute, Futian, Shenzhen, China*

(Received 25 July 2022; accepted 28 October 2022; published 14 November 2022)

In this work, we study the scale characteristics of the log- and outer-region motions and structures in subsonic and supersonic turbulence. To this end, a series of direct numerical simulations of the compressible turbulent channel flow at medium Reynolds numbers are performed. Based on this database, the streamwise and spanwise lengthscales of the outer-region motions are investigated by the two-point correlations and the one-dimensional spectra. The energy distribution among the multiscale structures in the outer region is found to be dominated by the semilocal friction-Reynolds-number effects rather than the Mach-number effects. This conclusion not only holds for the velocity fluctuations, but also the fluctuations of the thermodynamic variables. In addition, the streamwise and spanwise lengthscales of the outer motions do not alter significantly when the flow passes the sound barrier as reported by a previous experimental study [Bross, Scharnowski, and Kähler, J. Fluid Mech. **911**, A2 (2021)]. On the other hand, the self-similar structures populating the logarithmic region are investigated by adopting a linear coherence spectrum. The streamwise/wall-normal aspect ratio of the self-similar wall-attached structures of the streamwise velocity and temperature fluctuations is approximately 15.5 and the counterpart of density and pressure fluctuations is 1.8. The present study confirms the existence of self-similar structures in compressible wall turbulence and assesses their geometrical characteristics.

DOI: 10.1103/PhysRevFluids.7.114604

I. INTRODUCTION

Since the discovery of the streaks in the near-wall region of the turbulent boundary layers by Kline *et al*. [1], the coherent structures, as well as the energy-containing motions (eddies) in wall-bounded turbulence were extensively investigated over the past decades. Now, it is understood that, in addition to the streaks and the vortical structures residing in the near-wall region [1,2], there are also large-scale motions (LSMs), very-large-scale motions (VLSMs), and self-similar motions populating the logarithmic and outer regions. These three typical energy-containing motions were unmasked in high-Reynolds-number pipes [3,4], channels [5,6], and zero-pressure-gradient turbulent boundary layers [7,8]. In addition, they were also identified in compressible wall-bounded turbulence [9–11]. Further studies also revealed that these energy-containing motions not only exert pronounced influences on the near-wall turbulent intensities [12,13], but also the unsteadiness of the separated bubble downstream of the shockwave/boundary-layer interactions [14,15]. Thus, the

*Corresponding author: linfu@ust.hk

investigation of their physical characteristics has remarkable significance for drag reduction and flow-separation control of the high-speed vehicles. It should be noted that in internal flows, the long streaky low-streamwise-momentum motions are often referred to as "VLSMs," whereas in external flows they are more commonly referred to as "superstructures" [16]. In the present study, we do not differentiate between the two terminologies and denote these motions in internal/external flows as VLSMs collectively.

LSMs have a streamwise scale of approximately $1-2\delta$ (δ indicates the boundary thickness), and VLSMs are generally believed to extend several δ long along the streamwise direction (the exact length is disputed) and meander in the spanwise direction [16]. The investigations of the incompressible wall-bounded turbulence provided the majority of the knowledge concerning these motions. It is speculated that the coherent-structure organizations of compressible wall turbulence in the logarithmic and outer regions would resemble those of incompressible flows. However, this hypothesis is still controversial.

As early as 1989, Smits *et al*. [17] compared the turbulent structures of subsonic (Ma $= 0.1$, here Ma denotes the Mach number) and supersonic (Ma $= 2.9$) boundary layers, and found that their spanwise scales are almost identical, but the streamwise scales in the supersonic flow are about half the size of those in subsonic flow. Their analyses are based on the space-time correlations of the mass-flux fluctuations measured from the hot-wire (HW) probes. Smits and Dussauge [18] also summarized the experimental measurements (hot-wire measurements dominate) and came to the conclusion that the streamwise lengthscales of outer motions decrease obviously with increasing Mach number, whereas their spanwise scales have no statistical changes with the Reynolds and Mach numbers. However, Spina *et al*. [19] reported that the average spanwise extent of the largest eddies in a Mach 3 turbulent boundary layer is similar to that of subsonic turbulent boundary layers by adopting hot-wire and flow visualizations, whereas their average streamwise scales are about twice those of the low Reynolds number, subsonic turbulent boundary layers.

Nevertheless, these propositions are not totally in accordance with the measurement via particle image velocimetry (PIV). Ganapathisubramani *et al*. [9] used planar PIV to investigate the scale characteristics of the energy-containing motions in a Mach 2 turbulent boundary layer. By employing the two-point correlation, they discovered that the streamwise lengthscale of the streamwise velocity fluctuations at the outer region is nearly four-times as long as that in incompressible cases, and their spanwise lengthscale is slightly larger than that of the subsonic flow. However, Williams *et al*. [20] also investigated a hypersonic turbulent boundary layer at Mach 7.5 by PIV, and their conclusion was different, e.g., the streamwise correlation lengths are less sensitive to the compressibility. Very recently, Bross *et al*. [11] examined a sequence of compressible turbulent boundary layers varying from subsonic to supersonic by using planar two-dimensional (2-D) PIV and stereo-PIV, and they observed that there is a scale expansion in both streamwise and spanwise directions when flow passes the sound barrier. It is interesting to note that, rather than the absolute value of the Mach number, whether this phenomenon takes place relies on whether the flow speed is sub or supersonic.

Direct numerical simulation (DNS) is another tool to tackle this question. However, the findings from DNS diverge significantly from those of the aforementioned experimental studies. Ringuette *et al*. [21] performed a DNS study of a Mach 3 turbulent boundary layer and found that VLSMs in the compressible flow are similar to those in incompressible cases and their lengthscale is mostly shaped by the Reynolds-number effects. Pirozzoli and Bernardini [22] analyzed the structural organization of a Mach 2 turbulent boundary layer and reported that their streamwise lengthscales are identical to the incompressible cases, whereas the spanwise lengthscales are slightly larger. Later, they also observed that the spanwise lengthscales of the motions in the outer region of the Mach 1.5 turbulent channel flows are close to the incompressible flows [10]. The scale invariance of LSMs in supersonic wall turbulence was drawn in a series of works of their group and collaborators [10,22–24]. Recently, similar results were also provided by Yao and Hussain [25] and Huang *et al*. [26] after examining their own DNS database of compressible channel flows and supersonic/hypersonic turbulent boundary layers with different thermal boundary conditions. The later study also revealed

TABLE I. Summary of the experimental and numerical studies on the lengthscales of the outer-region motions in compressible wall-bounded turbulence. Here, TBL, CP, and CH denote the turbulent boundary layer, Couette-Poiseuille flow, and channel flow, respectively. λ_x and λ_z denote the streamwise and spanwise lengthscales, respectively. The symbols $\nearrow$ and $\searrow$ denote larger and smaller than the incompressible/subsonic counterparts, respectively, whereas $\rightarrow$ denotes no change.

Reference	Year	Flow	Ma	Method	λ_x	λ_z	Note
Smits *et al*. [17]	1989	TBL	0.1–2.9	HW	$\searrow$	$\rightarrow$	None
Spina *et al*. [19]	1994	TBL	3	HW	$\nearrow$	$\rightarrow$	None
Smits and Dussauge [18]	2006	TBL	0.035–11	HW	$\searrow$	$\rightarrow$	HW dominant
Ganapathisubramani *et al*. [9]	2006	TBL	2.0	PIV	$\nearrow$	$\nearrow$	None
Williams *et al*. [20]	2018	TBL	7.5	PIV	$\rightarrow$	None	None
Bross *et al*. [11]	2021	TBL	0.3–3	PIV	$\nearrow$	$\nearrow$	Transonic expansion
Pirozzoli and Bernardini [22]	2011	TBL	2	DNS	$\rightarrow$	$\nearrow$	None
Pirozzoli [23]	2012	TBL/CP	0.3–4	DNS	None	$\rightarrow$	None
Modesti and Pirozzoli [10]	2016	CH	0.1–3	DNS	None	$\rightarrow$	None
Yao and Hussain [25]	2020	CH	0–1.5	DNS	$\rightarrow$	$\rightarrow$	None
Huang *et al*. [26]	2022	TBL	2.5–10.9	DNS	$\rightarrow$	$\rightarrow$	None
Cogo *et al*. [24]	2022	TBL	2–5.86	DNS	None	$\rightarrow$	None

that the wall cooling condition plays a minor role in shaping the lengthscales of LSMs and VLSMs. Table I summarizes the experimental and numerical studies on the lengthscales of the outer-region motions in compressible wall-bounded turbulence. Reviewing the works of predecessors, it can be found that the scale characteristics of the motions in the outer region of the compressible wall turbulence are ambiguous from the experimental and numerical sides. Most of the DNS studies hold the view that their lengthscales are not sensitive to compressibility, whereas for the experimental studies, it has been a question of different opinions.

On the other hand, it is documented that there are self-similar motions populating the logarithmic region of the wall turbulence [27–30]. According to the well-known attached-eddy model, the logarithmic region is occupied by an array of self-similar energy-containing motions (or eddies) with their roots attached to the near-wall region [31,32]. Hence, examining the geometrical features of these self-similar structures is beneficial for both developing the attached-eddy hypothesis and advancing the knowledge of turbulent dynamics. In this respect, nearly all the works concentrated on incompressible wall-bounded turbulence. For example, Baars *et al*. [27] identified the self-similar structures of the streamwise velocity fluctuations in incompressible boundary layers by a linear coherence spectrum and found the streamwise/wall-normal aspect ratio (AR) of them is roughly 14. This scale characteristic was then employed to construct a filter for isolating the spectral energy results from the wall-attached eddies [33]. Will it still hold in compressible turbulence? Will the thermodynamic variables bear the same self-similar characteristics as the streamwise velocity fluctuations? If yes, what is their AR? None of these issues have been thoroughly investigated. Very recently, Yu *et al*. [34] employed the proper orthogonal decomposition to identify the self-similar structures of the streamwise velocity and the temperature fluctuations in a compressible channel flow, but their geometrical characteristics have not been clarified.

The work of the present study is divided into two parts. In the first part, we conduct a series of DNSs of the subsonic and the supersonic turbulent channel flows at medium Reynolds numbers (the maximal friction Reynolds number is 1150). Then, in conjunction with the open-source incompressible data, the Mach-number effects on the scale characteristics of the outer-region motions are dissected, together with the scale characteristics of the thermodynamic variables, such as p' (pressure fluctuation), T' (temperature fluctuation), and ρ' (density fluctuation). Particular attention is paid to the scale expansion when flow passes the sound barrier reported by a recent study [11]. In the second part, we elaborate on the geometrical characteristics of the self-similar

structures populating the logarithmic region. We generalize the work of Baars *et al*. [27] to the compressible flows by leveraging the database setup in the present study. We not only compare the geometrical properties of the self-similar wall-attached velocity fluctuation with the incompressible counterparts, but also unravel those of the thermodynamic variables. The present work may help develop an advanced scale-resolving method for predicting the compressible wall-bounded flows [35,36].

The focuses of the present study are summarized as follows.

(1) The scale characteristics of the outer-region motions in subsonic and supersonic wall turbulence are presented, not only for the velocity fluctuations, but also the fluctuations of the thermodynamic variables. The scale characteristics of the thermodynamic variables have rarely been reported before. Particular attention is paid to the scale expansion when flow passes the sound barrier reported by a recent study [11].

(2) The possible factors that may account for the differences between the experimental and numerical studies are presented, such as the variable for study, the method to normalize the spectrum, and the wall-normal position of the detected plane.

(3) The scale characteristics of the self-similar structures in the logarithmic region, not only for the streamwise velocity fluctuations, but also the thermodynamic variables are shown.

The paper is organized as follows. In Sec. II, the DNS setup and numerical validation are provided in detail. The scale characteristics of the outer-region motions in a compressible channel flow are analyzed by the two-point correlation and the one-dimensional spectrum in Sec. III, concurrently, the geometrical characteristics of the self-similar structures in the logarithmic region are also investigated in this section. Conclusions are given in Sec. IV.

II. NUMERICAL SETUP AND VALIDATION

DNSs of compressible turbulent channel flows were conducted with a finite-difference code by solving the three-dimensional unsteady compressible Navier-Stokes equations. The convective terms are discretized with a seventh-order upwind-biased scheme, and the viscous terms are evaluated with an eighth-order central difference scheme. Time advancement is performed using the third-order strong-stability-preserving (SSP) Runge-Kutta method [37]. A constant molecular Prandtl number Pr of 0.72 and a specific heat ratio γ of 1.4 are employed. The dependence of dynamical viscosity μ on temperature T is given by Sutherland's law, i.e.,

$$\mu = \mu_0 \frac{T_0 + S}{T + S} \left(\frac{T}{T_0} \right)^{3/2}, \tag{1}$$

where $S = 110.4\,\mathrm{K}$ and $T_0 = 273.1\,\mathrm{K}$.

All the DNSs are carried out in a rectangular box with its sizes along the streamwise (x), spanwise (z), and wall-normal (y) directions denoted as L_x, L_z, and L_y, respectively. In the streamwise and spanwise directions, the mesh is uniformly spaced, whereas, in the wall-normal direction, the mesh is hyperbolically clustered towards the walls. The isothermal no-slip conditions are imposed at the top and bottom walls, and the periodic boundary condition is imposed in the wall-parallel directions, i.e., the x and z directions. All simulations begin with a parabolic velocity profile with random perturbations superimposed and uniform temperature and density values. A body force is imposed in the streamwise direction to maintain a constant mass flow rate and a corresponding source term is also added in the energy equation [38].

In the present study, we carry out two simulations at a bulk Mach number $M_b = U_b/C_w = 0.8$ (U_b is the bulk velocity and C_w is the speed of sound at wall temperature) and $\mathrm{Re}_b = \rho_b U_b h/\mu_w = 7667$ and 17 000 (ρ_b denotes the bulk density, h the channel half-height, and μ_w the dynamic viscosity at the wall). Two other DNSs at a bulk Mach number $M_b = 1.5$ and $\mathrm{Re}_b = 9400$ and 20 020 are also conducted. For all cases, the computational domain has the same dimensions, namely, $L_x \times L_z \times L_y = 4\pi h \times 2\pi h \times 2h$. Previous studies verified that these setups of dimensions can capture most of the large-scale motions in the outer region of the boundary layer [39,40]. Details of the

TABLE II. Parameter settings of the compressible DNS database. Here, M_b denotes the bulk Mach number. Re_b, Re_τ, and Re_τ^* denote the bulk Reynolds number, friction Reynolds number, and semilocal friction Reynolds number, respectively. Δx^+ and Δz^+ denote the streamwise and spanwise grid resolutions in viscous units, respectively. $\Delta y^+_{\mathrm{min}}$ and $\Delta y^+_{\mathrm{max}}$ denote the finest and the coarsest resolution in the wall-normal direction, respectively. Tu_τ/h indicates the total eddy turnover time used to accumulate statistics.

Case	M_b	Re_b	Re_τ	Re_τ^*	Δx^+	Δz^+	$\Delta y^+_{\mathrm{min}}$	$\Delta y^+_{\mathrm{max}}$	Tu_τ/h
Ma08Re8K	0.8	7667	436	382	10.8	6.9	0.44	5.4	49.4
Ma08Re17K	0.8	17 000	882	778	10.8	6.5	0.63	6.4	15.3
Ma15Re9K	1.5	9400	594	395	7.3	3.7	0.5	5.9	30.2
Ma15Re20K	1.5	20 020	1150	780	9.3	4.7	0.49	6.9	9.1

parameter settings are listed in Table II. Two incompressible cases at $\mathrm{Re}_\tau = 547$ and $\mathrm{Re}_\tau = 934$ by Del Álamo and Jiménez [5] and Del Álamo *et al.* [41] are also employed for comparison. Details of the parameter settings are listed in Table III.

Both the Reynolds (denoted as $\bar{\phi}$) and the Favre-averaged (denoted as $\widetilde{\phi} = \overline{\rho\phi}/\overline{\rho}$) statistics are used in the present study. The corresponding fluctuating components are represented as ϕ' and ϕ'', respectively. Hereafter, we use the superscript $+$ to represent the normalization with the friction velocity (denoted as u_τ, $u_\tau = \sqrt{\tau_w/\rho_w}$, τ_w is the mean wall-shear stress) and the viscous lengthscale (denoted as δ_ν, $\delta_\nu = \nu_w/u_\tau$, $\nu_w = \mu_w/\rho_w$). We also use the superscript $*$ to represent the normalization with the semilocal wall units, i.e., $u_\tau^* = \sqrt{\tau_w/\overline{\rho}}$ and $\delta_\nu^* = \overline{\nu(y)}/u_\tau^*$. Hence, the relationship between the semilocal friction Reynolds number and the friction Reynolds number is $\mathrm{Re}_\tau^* = \mathrm{Re}_\tau\sqrt{(\overline{\rho_c}/\bar{\rho}_w)}/(\overline{\mu_c}/\bar{\mu}_w)$. The subscript c refers to the quantities evaluated at the channel center. It is noted that the cases Ma08Re8K and Ma08Re17K share similar Re_τ^* with the cases Ma15Re9K and Ma15Re20K, respectively. To verify the compressible dataset of present study, Fig. 1 compares the DNS results of Ma08Re8K and Ma08Re17K with the flow statistics of Yao and Hussain [25] at identical Ma_b and Re_b, respectively. Both the mean quantities and the Reynolds stress $\tau_{ij} = \bar{\rho}R_{ij}$ with $R_{ij} = \widetilde{u_i''u_j''} = \widetilde{u_iu_j} - \widetilde{u}_i\widetilde{u}_j$ (v and w denote the wall-normal and spanwise velocity, respectively) are compared. Figure 2 compares the mean quantities and the root-mean-square (r.m.s.) of the velocity fluctuations of Ma15Re9K and Ma15Re20K with the results reported by Modesti and Pirozzoli [10] at $M_b = 1.5$, $\mathrm{Re}_b = 7667$ and $M_b = 1.5$, $\mathrm{Re}_b = 17\,000$, respectively. All the profiles of the concerned quantities agree reasonably with the previous studies. The minor differences shown in Fig. 2 are ascribed to the distinctions in Re_b. All these confirm the accuracy of the present database.

Figure 3 plots the variations of the mean local Mach number (M_l) as functions of the wall-normal height y/h. For the cases at $M_b = 0.8$, $M_l \approx 0.69$ at $y = 0.2h$, whereas for the cases at $M_b = 1.5$, $M_l \approx 1.16$ at the same wall-normal height. Considering that $y = 0.2h$ is the upper bound of the logarithmic region [42], dissecting the scale characteristics at this wall-normal height can shed light on the differences between the large-scale motions in the subsonic and supersonic wall-bounded turbulence. The results presented below are mainly focused on this wall-normal position. We also show that the conclusions drawn below are not changed with varying wall-normal heights within the outer region (see the Appendix).

TABLE III. Parameter settings of the incompressible DNS database.

Case	Re_τ	Re_τ^*	$L_x(h)$	$L_y(h)$	$L_z(h)$	Δx^+	Δz^+	$\Delta y^+_{\mathrm{min}}$	$\Delta y^+_{\mathrm{max}}$	Tu_τ/h
Ma00Re10K	547	547	8π	2	4π	13.4	6.8	0.04	6.7	22
Ma00Re18K	934	934	8π	2	3π	11.5	5.7	0.03	7.6	12

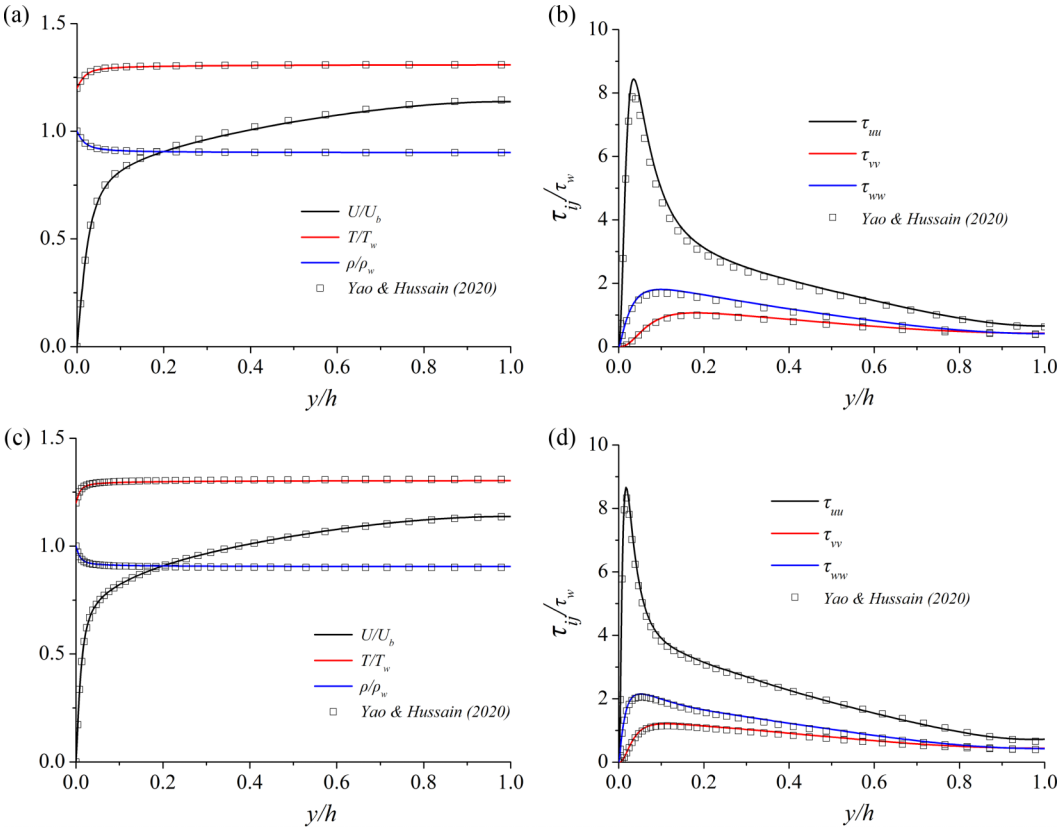

FIG. 1. Profiles of mean streamwise velocity, mean temperature, and mean density for the cases (a) Ma08Re8K and (c) Ma08Re17K; profiles of the Reynolds stress for the cases (b) Ma08Re8K and (d) Ma08Re17K. The profiles of T/T_w are shifted upward by $\Delta(T/T_w) = 0.2$ for better comparison.

III. RESULTS AND DISCUSSIONS

A. Variable for characterizing outer-layer motions

Before processing our analysis, it is crucial to clarify which physical variable is appropriate to characterize the scales of the outer-layer motions. Several variables were employed by previous studies to scrutinize the scale characteristics of compressible wall-bounded turbulence. For example, Smits *et al.* [17] adopted the correlated signals of the mass-flux fluctuations $(\rho u)'$ to depict the spatial organizations of the coherent structures in the compressible boundary layers. Ganapathisubramani *et al.* [9] used the two-point correlation of u' to measure the lengthscale of VLSMs in a turbulent boundary layer of Mach 2. Moreover, $\sqrt{\rho}u''$ was also visualized to display the formation of the energy-containing motions vividly [25,26,43].

In this study, the behaviors of these quantities are compared by utilizing the streamwise and spanwise two-point correlations based on the case Ma15Re20K. For the streamwise two-point correlation of variable ψ, it takes the form of

$$R_x(r_x, y) = \frac{\langle \psi(x, y, z)\psi(x + r_x, y, z)\rangle}{\langle \psi^2 \rangle}, \tag{2}$$

where r_x is the separation distance along the streamwise direction and $\langle\cdot\rangle$ represents the averaging in the temporal and spatially homogeneous directions. The spanwise two-point correlation R_z can be defined in a similar way. Figures 4(a) and 4(b) show the variations of the streamwise and spanwise

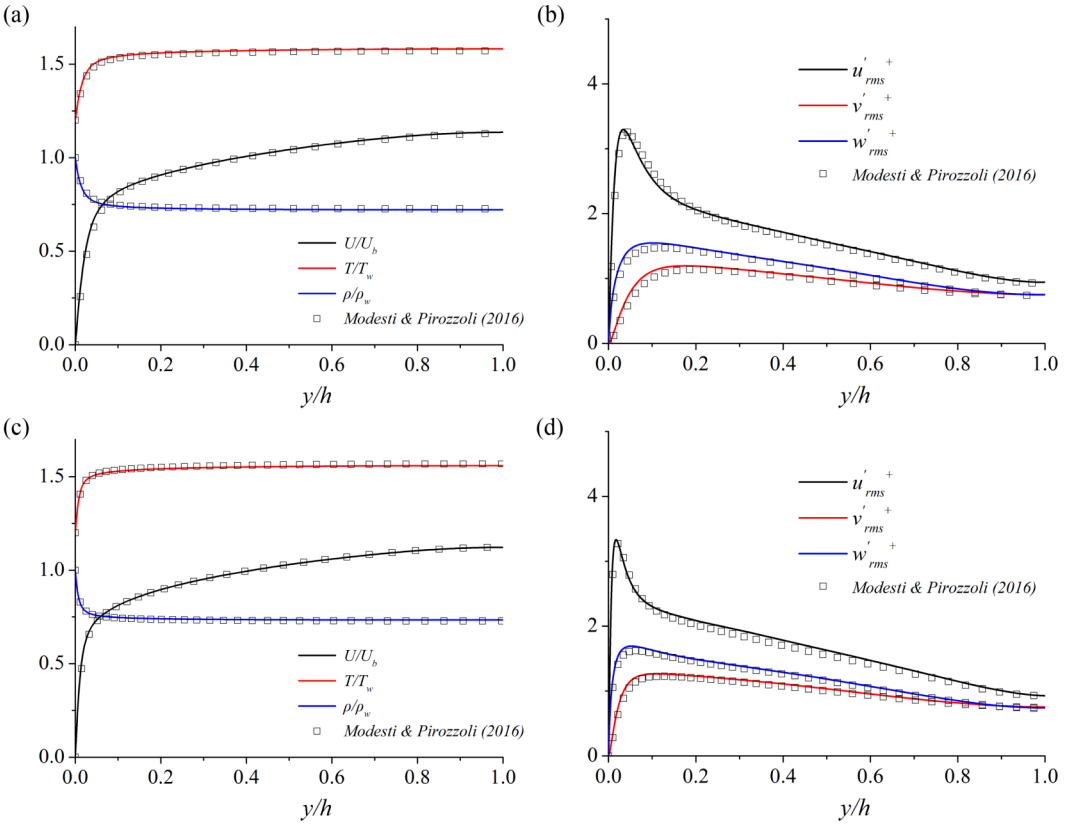

FIG. 2. Profiles of mean streamwise velocity, mean temperature, and mean density for the cases (a) Ma15Re9K and (c) Ma15Re21K; profiles of the root-mean-square of the velocity fluctuation for the cases (b) Ma15Re9K and (d) Ma15Re21K. The profiles of T/T_w are shifted upward by $\Delta(T/T_w) = 0.2$ for better comparison.

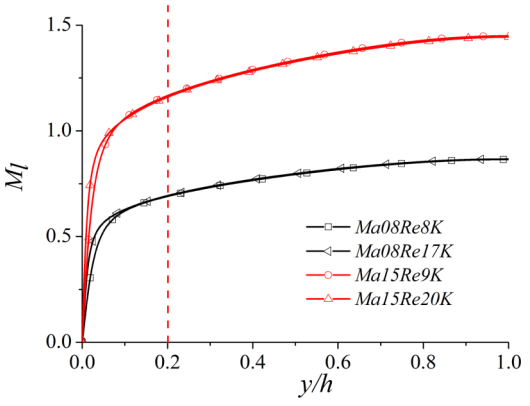

FIG. 3. Profiles of mean local Mach number for all compressible cases. The red dashed line indicates $y = 0.2h$, i.e., the wall-normal position for investigation in the present study.

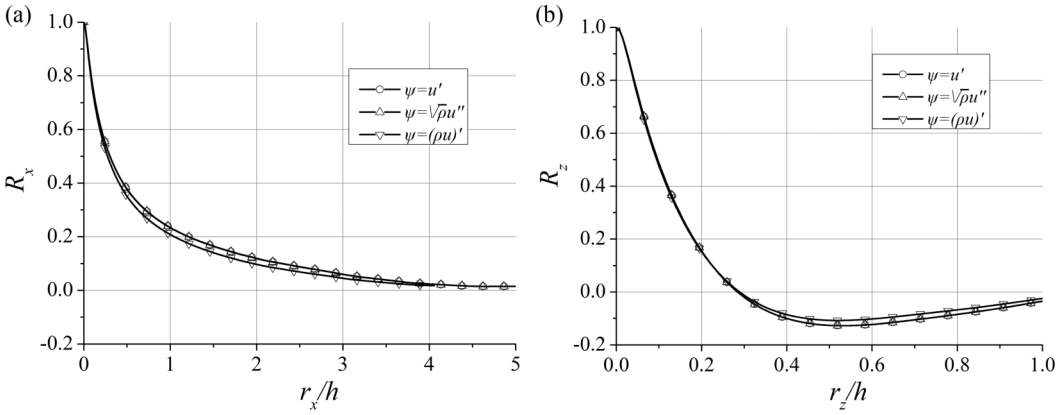

FIG. 4. (a) Streamwise and (b) spanwise two-point correlations of u', $\sqrt{\rho}u''$, and $(\rho u)'$ for the case Ma15Re20K at $y/h = 0.2$.

two-point correlations of the above-mentioned variables at $y = 0.2h$, respectively. We only show the profiles at $r_x > 0$ and $r_z > 0$ due to the symmetries of the two correlations with respect to $r_x = 0$ and $r_z = 0$, respectively. It can be seen that the profiles of R_x and R_z of all the quantities overlap with each other well. We checked that the same conclusion applies to other velocity fluctuation components and the assessment is not shown here for brevity. It indicates that these physical quantities share identical lengthscale characteristics statistically, at least when $M_b \leqslant 1.5$. It also agrees with the observation of Ringuette *et al.* [21] who reported that the correlations of $(\rho u)'$ and u' are very similar in a turbulent boundary layer at Mach 3. Whether it holds at higher Mach numbers remains to be checked. Thus, the results presented below mainly focus on the variables weighted by $\sqrt{\rho}$.

B. Large-scale motions in subsonic and supersonic turbulent channel flows

1. Density-weighted velocity fluctuations

In this section, we dedicate it to comparing the scale characteristics of the large-scale motions in subsonic and supersonic channel flows. Figures 5(a) and 5(b) show the premultiplied streamwise and spanwise spectra of the density-weighted streamwise velocity fluctuations ($\sqrt{\rho}u''$) at $y = 0.2h$. The area under the spectral curve represents the intensity of the density-weighted Reynolds stress $\overline{(\sqrt{\rho}u'')^2}$. For the streamwise spectra, all the spectra peak at $\lambda_x \approx 2h$ and no observable differences in the streamwise wavelengths of the most energetic scales ($\lambda_{x,me}$) between the incompressible, subsonic, and supersonic cases can be found. The spectral energy of the peaks is determined by the magnitude of Re_τ^* instead. For the spanwise spectra, all the cases peak at $\lambda_z \approx 1h$, the typical width of VLSMs [42], and the distinctions between the $\lambda_{z,me}$ of all cases are still inconspicuous. Similar conclusions about the lengthscales of $\sqrt{\rho}u''$ in the outer region were also been drawn by the authors of [25].

Very recently, Bross *et al.* [11] conducted an experimental study and observed that the $\lambda_{x,me}$ in the outer region of the supersonic turbulent boundary layers were slightly larger than those of the subsonic cases, whereas the $\lambda_{z,me}$ of the supersonic cases have a distinct increase compared with the subsonic cases. In compressible turbulent channel flows, at least within the Reynolds and Mach numbers under scrutinizing by the present study, this phenomenon is not that remarkable. The possible explanations are given in Sec. III B 3. As a side note, Bross *et al.* [11] normalized the spectra of the streamwise velocity fluctuations in a different way, i.e., $(\overline{\rho}/\rho_w)k_xE_{u'u'}/u_\tau^2$ and $(\overline{\rho}/\rho_w)k_zE_{u'u'}/u_\tau^2$. We verified that the conclusions reached above are unaffected by normalizing the spectra in this manner (see Sec. III B 3).

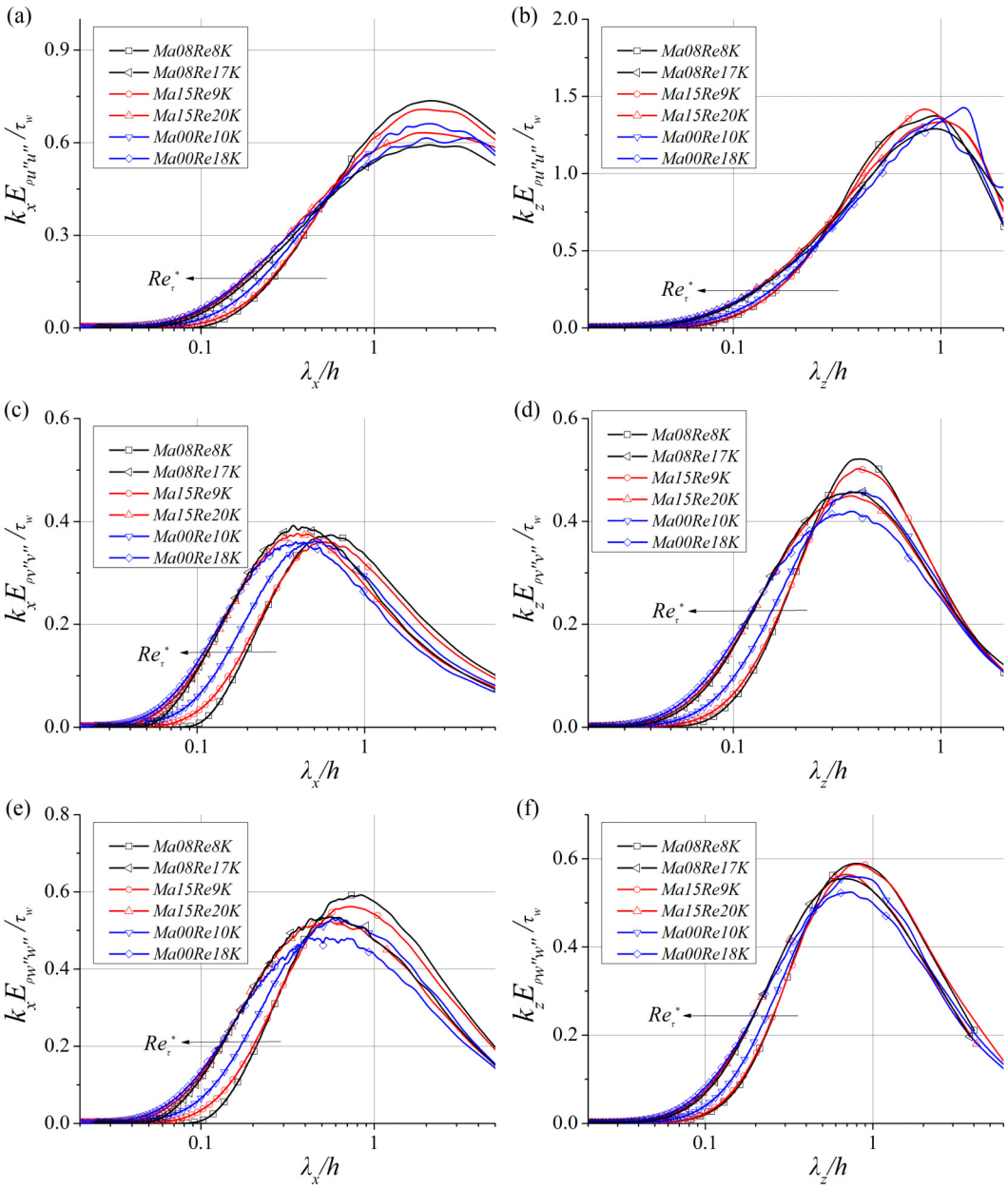

FIG. 5. (a), (c), (e) Streamwise and (b), (d), (f) spanwise premultiplied one-dimensional spectra of (a,b) $\sqrt{\rho}u''$, (c,d) $\sqrt{\rho}v''$, (e,f) and $\sqrt{\rho}w''$ for all cases at $y/h = 0.2$.

The premultiplied streamwise and spanwise spectra of $\sqrt{\rho}v''$ and $\sqrt{\rho}w''$ are also shown in Figs. 5(c)–5(f), respectively. It can be seen that no clear Mach-number dependence of the wavelengths of the spectral peaks can be identified for all cases, regardless of the spectral direction. Moreover, the spectra of the cases at larger Re_τ^* are more energetic in small lengthscales and the cases at similar Re_τ^* collapse well. Although less obvious, this phenomenon can also be seen in the premultiplied streamwise and spanwise spectra of $\sqrt{\rho}u''$. These observations highlight the fact

that the semilocal Reynolds-number effects dominate the energy distribution among the multiscale eddies in the outer region, regardless of whether the flow passes the sound barrier or not, and whether the flow is compressible or not. They are also consistent with some previous studies [43–47], which emphasized that the semilocal Reynolds number Re_τ^* is a key similarity parameter for the compressible wall-bounded turbulence. In summary, the present study does not observe that there is a sudden increase in lengthscales of the out-layer motions when the flow transitions from subsonic to supersonic state.

2. Thermodynamic variables

In this section, we turn to report the scale characteristics of the thermodynamic variables, i.e., T', p', and ρ' at outer region $y = 0.2h$. Figures 6(a)–6(f) show the premultiplied streamwise and spanwise spectra of T', p', and ρ' of the compressible cases, respectively. All the spectra are normalized by their maximum values for comparison. It is apparent that the cases with similar Re_τ^* share akin scale-dependent energy distributions for all three thermodynamic variables. This observation supports the viewpoint put forward above that Re_τ^* is the key parameter in shaping the spectra. Moreover, no clear Mach-number effects on the scale characteristics can be identified between the cases with similar Re_τ^*. This demonstrates once again that there is no sudden increase in lengthscales of the outer-region motions when the flow becomes supersonic from a subsonic state, as the scale characteristics of the thermodynamic variables are highly linked with those of LSMs and VLSMs [22].

3. Discussions

The reason why the DNS results differ from the experimental results merits a discussion. Ganapathisubramani *et al.* [9] and Bross *et al.* [11] conjectured that analysis of mass-flux $(\rho u)'$ versus u' may result in distinct conclusions about the lengthscales of the outer motions. The origin of this discrepancy is ascribed to the different velocity measurement tools in the experiments, i.e., the hot wire versus the PIV. However, Fig. 4 demonstrates that the discrepancies of the mean lengthscale between these two variables at $y = 0.2h$ are minor, at least, within the Reynolds and Mach numbers under consideration. Figure 7 compares the streamwise and spanwise spectra of the streamwise velocity fluctuations for Ma15Re9K and Ma15Re20K with different density-weighting approaches and without density weighting. It is noted that $(\overline{\rho}/\rho_w)k_xE_{u'u'}/u_\tau^2$ and $(\overline{\rho}/\rho_w)k_zE_{u'u'}/u_\tau^2$ are commonly adopted by experimental studies to exhibit the scale characteristics of the velocity signals. It can be seen that the density-weighted spectra overlap with each other. It indicates that the different weighting methods do not alter the energy distributions among scales within the Reynolds and Mach numbers under consideration. In addition, though the spectra without density weighting have unique forms, the lengthscales of their peaks are consistent with the density-weighted ones, that is, $\lambda_{x,e} \approx 2h$ and $\lambda_{z,e} \approx 1h$. In other words, for the spectra of the current examples under examination, the consequences of weighting with density on the values of $\lambda_{x,e}$ and $\lambda_{z,e}$ are negligible.

Another possible reason is that the configuration of the wall turbulence here is different from that of the work of experimentalists, who usually investigated the lengthscales of outer motions in turbulent boundary layers instead of channel flow [9,11,17,48]. Some previous studies on incompressible wall turbulence reported that the average streamwise lengthscale of VLSMs in internal flow (e.g., pipe and channel flow) was larger than that of the turbulent boundary layer [8,49,50]. In addition, the friction Reynolds numbers of the cases in the present study are $O(10^2)$ to $O(10^3)$, whereas for the works of experimentalists, they are usually $O(10^3)$ to $O(10^4)$ [9,11]. Hence, the observations reported in the present study remain to be verified in high-Reynolds-number wall turbulence. We also notice that, in the experiments conducted by Bross *et al.* [11], the walls were hot (the wall temperature was higher than that of free stream), whereas for the turbulent channel flows in the present study, the walls are cool (see Figs. 1 and 2). This might be another nonnegligible factor.

At last, the wall-normal location of the measurement plane deserves a discussion. When examining the spanwise lengthscales of the outer motions, Bross *et al.* [11] set the measurement plane

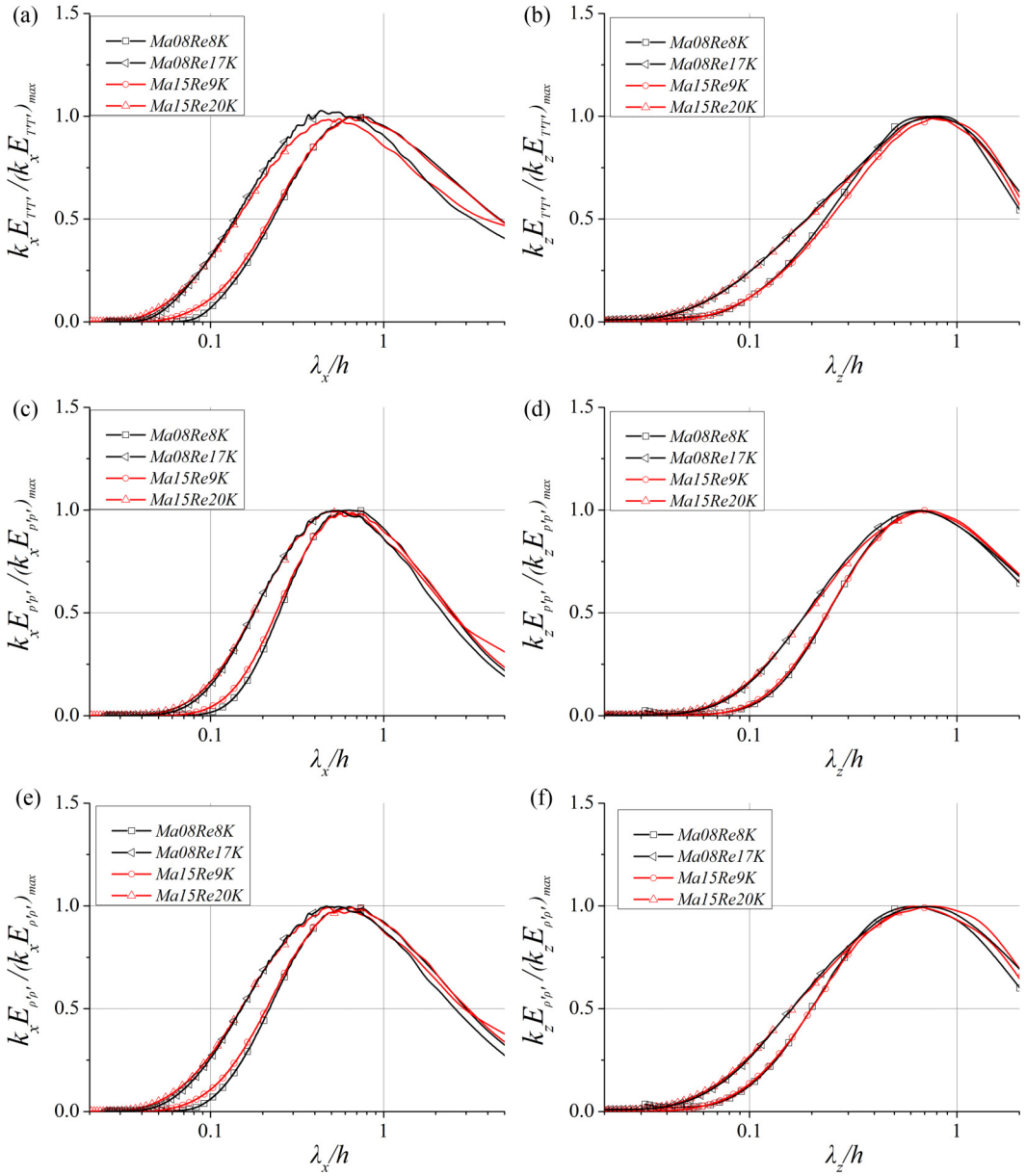

FIG. 6. (a), (c), (e) Streamwise and (b), (d), (f) spanwise premultiplied one-dimensional spectra of (a), (b) T', (c), (d) p', and (e), (f) ρ' for all compressible cases at $y/h = 0.2$. All the spectra are normalized by their maximum values.

at approximately $y/\delta = 0.1$ for the subsonic cases and at $y/\delta = 0.2$ for the supersonic cases. They found that the average width of the outer motions was larger for the supersonic cases. In Fig. 8, we repeated this process, and compared the spanwise spectra of $\sqrt{\rho}u''$ for different cases. A similar phenomenon can also be observed. However, as the spanwise lengthscales of the energy-containing motions populating the logarithmic and outer regions scale in the outer unit and increase with their wall-normal heights [41,51,52], the discrepancies of $\lambda_{z,e}$ for the supersonic and the subsonic cases

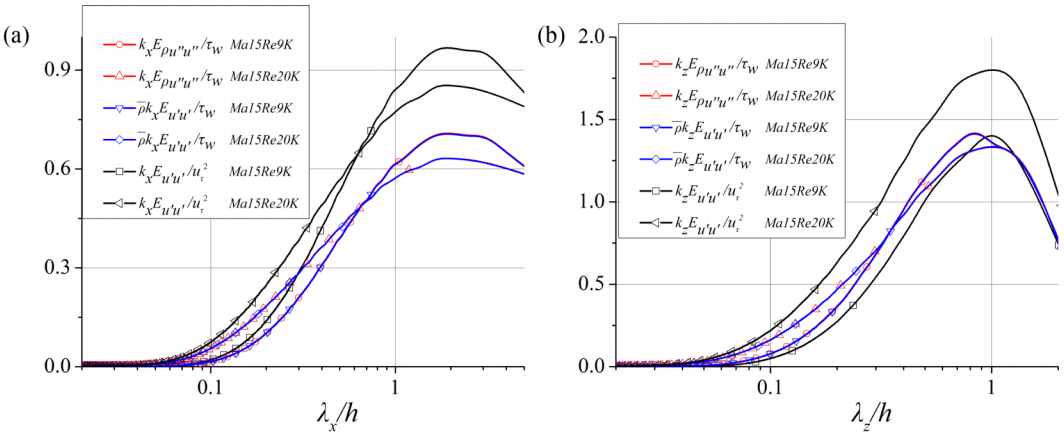

FIG. 7. (a) Streamwise and (b) spanwise premultiplied spectra of the streamwise velocity fluctuations for Ma15Re9K and Ma15Re20K at $y = 0.2h$ with different density-weighted approaches and without density weighting.

shown in Fig. 8 here and Fig. 15 of [11] are ascribed to the wall-normal growth of the motions rather than the Mach-number effects. Thus, to preclude the scale-growth effects and uncover the Mach-number effects on lengthscales of LSMs and VLSMs, the wall-normal position of the measurement planes for the supersonic and the subsonic cases should be identical and located in the logarithmic or outer regions.

C. Self-similar structures in compressible turbulent channel flows

In this section, we pay attention to the self-similar structures in compressible turbulent channel flows. To inspect the structures that are highly correlated with the near-wall flows, the linear coherence spectrum (LCS) of the variable ψ is adopted, which is given by

$$\gamma^2(y_o, y; \lambda_x) \equiv \frac{|\langle \widehat{\psi}(y_o; \lambda_x)\widehat{\psi}^*(y; \lambda_x)\rangle|^2}{\langle|\widehat{\psi}(y_o; \lambda_x)|^2\rangle\langle|\widehat{\psi}(y; \lambda_x)|^2\rangle}, \tag{3}$$

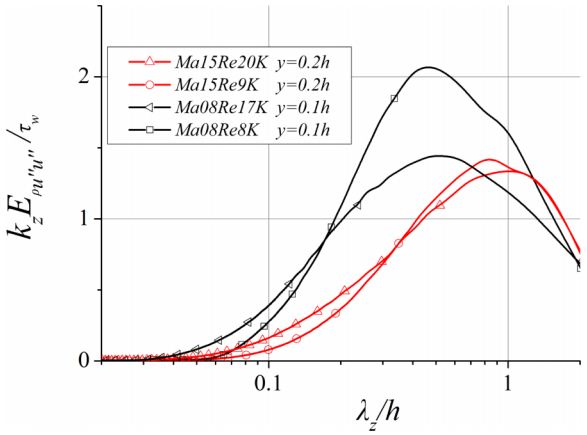

FIG. 8. Spanwise premultiplied spectra of $\sqrt{\rho}u''$ at $y = 0.1h$ for the subsonic cases and at $y = 0.2h$ for the supersonic cases.

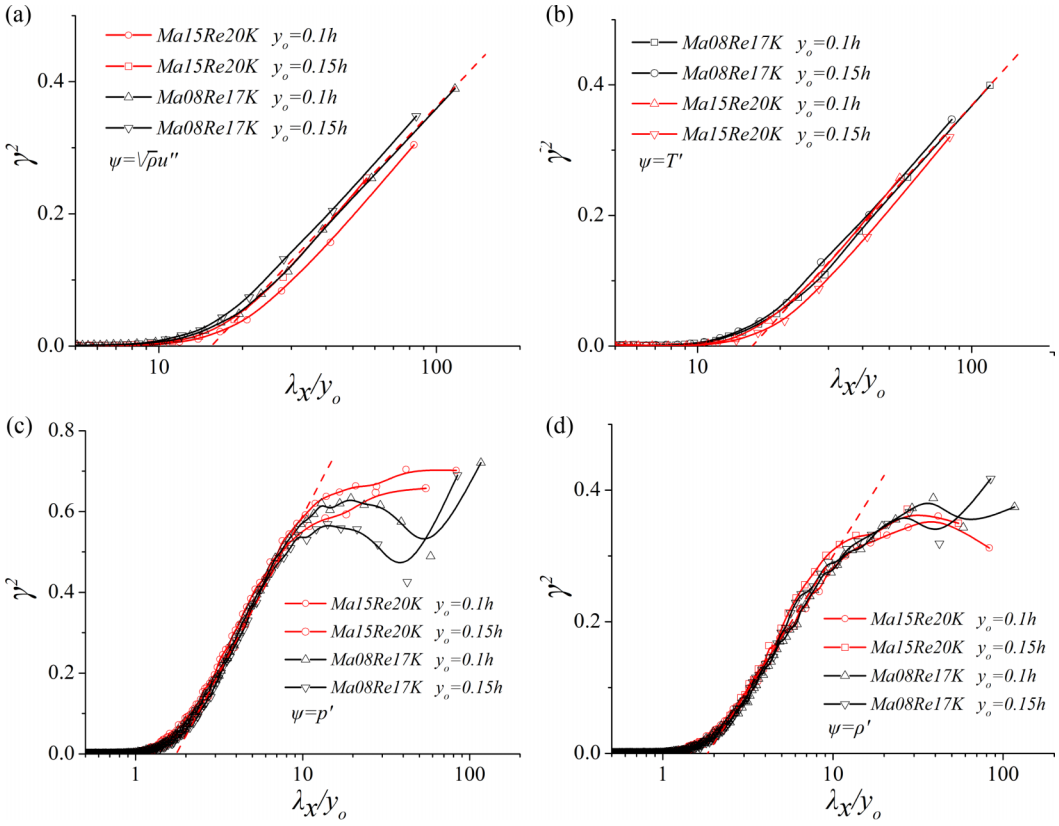

FIG. 9. Variations of γ^2 as functions of λ_x/y_o at two selected wall-normal heights, i.e., $y_o = 0.1h$ and $y_o = 0.15h$, for (a) $\psi = \sqrt{\rho}u''$, (b) T', (c) p', and (d) ρ', respectively. The dashed lines in the subfigures denote the logarithmic growth Eq. (4).

where $\psi(y_o)$ denotes the variable ψ at the location y_o in the logarithmic region, $\psi(y)$ denotes the variable ψ at the location y in the near-wall region, $\widehat{\psi}$ is the Fourier coefficient of ψ, $\widehat{\psi}^*$ is the complex conjugate of $\widehat{\psi}$, and $|\cdot|$ is the modulus. γ^2 evaluates the square of the scale-specific correlation between $\psi(y_o)$ and $\psi(y)$ with $0 \leqslant \gamma^2 \leqslant 1$ [53]. LCS was adopted to study the self-similar wall-attached structures in incompressible boundary layers [27,33] and the coherence between the temperature and the velocity fields in compressible wall turbulence [54]. To the authors' knowledge, no study on the geometrical characteristics of the self-similar structures in compressible turbulent channel flows by employing LCS has been reported, particularly the structures of the thermodynamic variables. In the present study, we fill this gap via analyzing the cases Ma08Re17K and Ma15Re20K, as their Reynolds numbers are relatively higher.

In the present study, the near-wall region is fixed at $y^+ \approx 0.6$ and the outer reference height y_o is located in the logarithmic region. We checked that, as long as $y^+ \leqslant 15$, the results presented below are insensitive to the choice of y^+. Figures 9(a) to 9(d) show the variations of γ^2 as functions of λ_x/y_o at two selected wall-normal heights, i.e., $y_o = 0.1$ and $y_o = 0.15$, for $\psi = \sqrt{\rho}u''$, T', p', and ρ', respectively. For $\psi = \sqrt{\rho}u''$ and T', γ^2 grows linearly with $\ln(\lambda_x/y_o)$ for $\lambda_x/y_o \geqslant 20$, whereas for $\psi = p'$ and ρ', the similar linear relations can be recognized for $2 \leqslant \lambda_x/y_o \leqslant 10$. Moreover, for the wall turbulence at different wall-normal heights and Mach numbers, the γ^2 profiles of a target variable ψ roughly coincide with each other in these regions. It indicates that there are self-similar structures of ψ populating the logarithmic region whose scale characteristics are not sensitive to the

TABLE IV. The fitted constants C_1, C_2 in Eq. (4) and the corresponding AR assessed by Eq. (5) for different ψ.

ψ	C_1	C_2	AR
$\sqrt{\rho}u''$	0.194	−0.531	15.44
T'	0.20	−0.552	15.79
p'	0.339	−0.190	1.75
ρ'	0.177	−0.107	1.83

Mach numbers. This scenario is consistent with the celebrated attached-eddy model [31,32], which hypothesizes that the energy-containing motions in the logarithmic region are self-similar and can permeate into the near-wall region.

The magnitude of γ^2 within the self-similar region takes the form of

$$\gamma^2 = C_1 \ln\left(\frac{\lambda_x}{y_o}\right) + C_2, \tag{4}$$

where C_1 and C_2 are two constants and can be estimated by fitting the γ^2 spectra over this range. Baars *et al*. [27] proposed that the streamwise/wall-normal aspect ratio of the self-similar structures can be assessed by

$$AR \equiv \left.\frac{\lambda_x}{y_o}\right|_{\gamma^2=0} = \exp\left(\frac{-C_2}{C_1}\right), \tag{5}$$

according to the hierarchical structure of the self-similar attached eddies [32]. The values of C_1, C_2, and AR for distinct ψ are listed in Table IV. It can be seen that the AR of $\sqrt{\rho}u''$ and T' are very close to each other and appropriately equal to 15.5. This result is in accordance with the assessment conducted by Baars *et al*. [27] who found the AR of the self-similar structures of the streamwise velocity fluctuations in incompressible turbulent boundary layers is 14. In addition, it is not unexpected that the AR of T' is closely approximate to that of $\sqrt{\rho}u''$, as a number of studies show that the strong Reynolds analogy (SRA) is valid in compressible wall turbulence [35,38,55,56]. For p' and ρ', the AR is approximately equal to 1.8 and significantly smaller than those of $\sqrt{\rho}u''$ and T'. This observation is reminiscent of the property of p' in incompressible wall turbulence, that is, p' is more energetic at small scales ($\lambda_x \leqslant C_3 h$, C_3 is a constant) [57]. Baars *et al*. [27] and Baars and Marusic [33] also noticed that the γ^2 spectra of u' in incompressible turbulent boundary layers tend to be constant at an outer-scaling limit of $\lambda_x/h \approx 10$. It cannot be observed by the present study for $\psi = \sqrt{\rho}u''$ and T' due to the limited size of the computational domain. However, for $\psi = p'$ and ρ', the γ^2 spectra shown in Figs. 9(c) and 9(d) departs from the power-law relation Eq. (4) for $\lambda_x/y_0 \geqslant 10$, which results from the very large-scale structures of these two variables. Again, this shows that the scale characteristics of p' and ρ' are completely different from those of $\sqrt{\rho}u''$ and T' in compressible wall turbulence.

Finally, we want to point out that the geometrical characteristics of the self-similar structures reported in the present study may aid in developing physics-based data-driven filters in compressible wall turbulence study, similar to the work of the authors of [33] in incompressible flows. In addition, the LCS employed here can also be used to shed light on the effects of the wall thermal boundary conditions on the sizes of the self-similar structures in the compressible flows. For example, Huang *et al*. [26] observed that strong wall cooling can lead to a remarkable reduction in the scale separation between the small and large eddies. The LCS can be developed as an effective tool to quantify this variation.

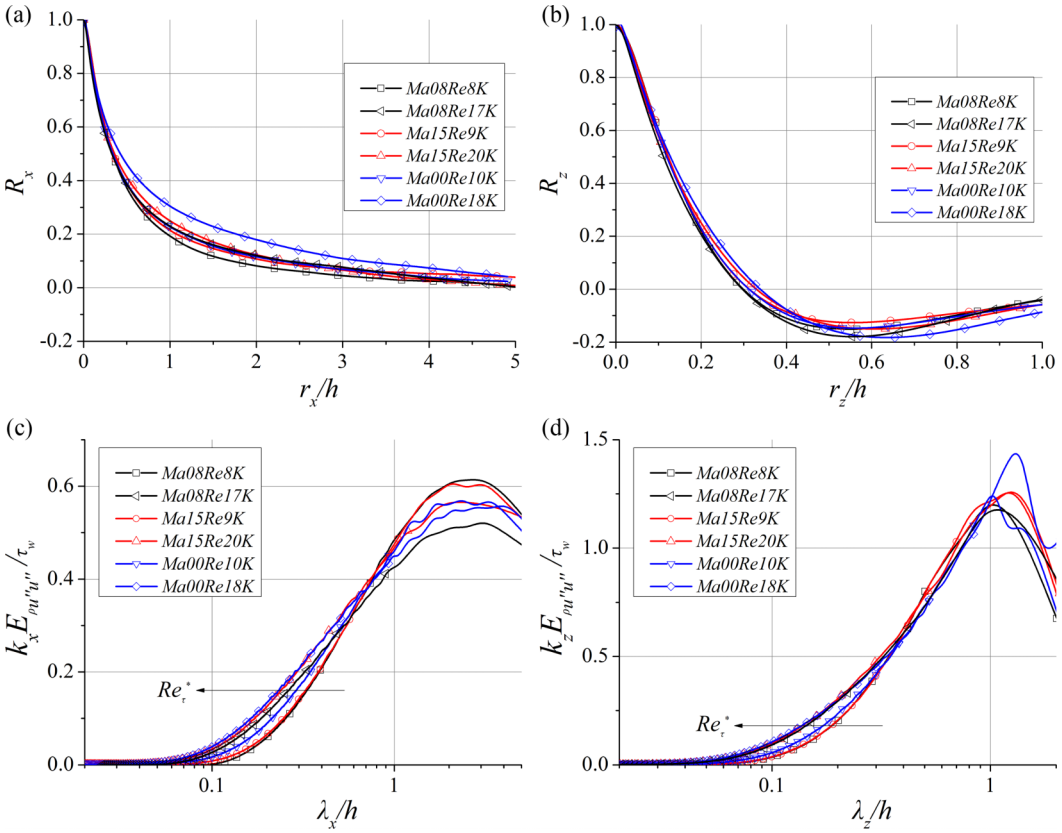

FIG. 10. (a) Streamwise and (b) spanwise two-point correlations of $\sqrt{\rho}u''$ for all cases at $y/h = 0.3$; (c) streamwise and (d) spanwise premultiplied one-dimensional spectra of $\sqrt{\rho}u''$ for all cases at $y/h = 0.3$.

IV. CONCLUSION

In the present study, we conduct a series of DNSs of the subsonic and supersonic turbulent channel flows at moderate Reynolds numbers. By employing the DNS database, we compare the scale characteristics of the outer motions in subsonic and supersonic turbulence and dissect the geometrical characteristics of the self-similar structures for the streamwise velocity fluctuations and the fluctuations of the thermodynamic variables. The conclusions are summarized below.

(i) The semilocal friction Reynolds number rather than the Mach number determines the energy distribution among the multiscale structures in the outer region not only for the velocity fluctuations, but also for the fluctuations of the thermodynamic variables. In addition, contrary to what a prior experimental study claimed, we did find that the streamwise and spanwise lengthscales of the outer motions alter significantly when flow passes the sound barrier.

(ii) The streamwise/wall-normal aspect ratio of the self-similar wall-attached structures of $\sqrt{\rho}u''$ and T' is 15.5, which is similar to that of the self-similar structures in incompressible wall turbulence. The counterpart of p' and ρ' is 1.8, which was not reported before. The very large-scale structures of p' and ρ' are those with $\lambda_x/y_0 \geqslant 10$. These scale characteristics are found to be not sensitive to the Mach and Reynolds numbers.

It is noted that the conclusions drawn here are only verified by the database of the compressible channel flows. Whether they hold in wall turbulence with different configurations requires further research. In addition, the wall temperature is deemed to impose nonnegligible effects on the

energy-containing motions in wall-bounded turbulence. Hence, it is of great significance to investigate them in turbulent boundary layers with different wall temperatures.

ACKNOWLEDGMENTS

We would like to thank Professor Jiménez for making the incompressible DNS data available. L.F. acknowledges the fund from the Research Grants Council (RGC) of the Government of Hong Kong Special Administrative Region (HKSAR) with RGC/ECS Project (No. 26200222), the fund from Guangdong Basic and Applied Basic Research Foundation (No. 2022A1515011779), and the fund from the Project of Hetao Shenzhen-Hong Kong Science and Technology Innovation Cooperation Zone (No. HZQB-KCZYB-2020083).

APPENDIX: SCALE CHARACTERISTICS AT OTHER WALL-NORMAL POSITION

Figure 10 shows the streamwise and spanwise two-point correlations and spectra of $\sqrt{\rho}u''$ at $y = 0.3h$ for all cases. For the two-point correlations, all the profiles nearly coincide (except the R_x of Ma0018K). For the spectra, the $\lambda_{x,me}$ of all cases is approximately equal to 2.5, whereas for $\lambda_{z,me}$, that is 1.2. Again, all these suggest that there is no recognizable scale expansion of the outer-region motions in both streamwise and spanwise directions when flow passes the sound barrier.

[1] S. Kline, W. Reynolds, F. Schraub, and P. Runstadler, The structure of turbulent boundary layers, J. Fluid Mech. **30**, 741 (1967).
[2] W. Schoppa and F. Hussain, Coherent structure generation in near-wall turbulence, J. Fluid Mech. **453**, 57 (2002).
[3] K. C. Kim, Very large-scale motion in the outer layer, Phys. Fluids **11**, 417 (1999).
[4] X. Wu, J. Baltzer, and R. Adrian, Direct numerical simulation of a 30R long turbulent pipe flow at $R^+ = 685$: large-and very large-scale motions, J. Fluid Mech. **698**, 235 (2012).
[5] J. C. Del Álamo and J. Jiménez, Spectra of the very large anisotropic scales in turbulent channels, Phys. Fluids **15**, L41 (2003).
[6] A. Lozano-Durán and J. Jiménez, Time-resolved evolution of coherent structures in turbulent channels: characterization of eddies and cascades, J. Fluid Mech. **759**, 432 (2014).
[7] J. Sillero, J. Jiménez, and R. Moser, One-point statistics for turbulent wall-bounded flows at Reynolds numbers up to $\delta^+ \approx 2000$, Phys. Fluids **25**, 105102 (2013).
[8] J. Sillero, J. Jiménez, and R. Moser, Two-point statistics for turbulent boundary layers and channels at Reynolds numbers up to $\delta^+ \approx 2000$, Phys. Fluids **26**, 105109 (2014).
[9] B. Ganapathisubramani, N. Clemens, and D. Dolling, Large-scale motions in a supersonic turbulent boundary layer, J. Fluid Mech. **556**, 271 (2006).
[10] D. Modesti and S. Pirozzoli, Reynolds and Mach number effects in compressible turbulent channel flow, Int. J. Heat Fluid Flow **59**, 33 (2016).
[11] M. Bross, S. Scharnowski, and C. Kähler, Large-scale coherent structures in compressible turbulent boundary layers, J. Fluid Mech. **911**, A2 (2021).
[12] R. Mathis, N. Hutchins, and I. Marusic, Large-scale amplitude modulation of the small-scale structures in turbulent boundary layers, J. Fluid Mech. **628**, 311 (2009).
[13] W. J. Baars, N. Hutchins, and I. Marusic, Spectral stochastic estimation of high-Reynolds-number wall-bounded turbulence for a refined inner-outer interaction model, Phys. Rev. Fluids **1**, 054406 (2016).
[14] B. Ganapathisubramani, N. Clemens, and D. Dolling, Low-frequency dynamics of shock-induced separation in a compression ramp interaction, J. Fluid Mech. **636**, 397 (2009).
[15] R. Baidya, S. Scharnowski, M. Bross, and C. Kähler, Interactions between a shock and turbulent features in a mach 2 compressible boundary layer, J. Fluid Mech. **893**, A15 (2020).

[16] A. Smits, B. McKeon, and I. Marusic, High–Reynolds number wall turbulence, Annu. Rev. Fluid Mech. **43**, 353 (2011).
[17] A. Smits, E. Spina, A. Alving, R. Smith, E. Fernando, and J. Donovan, A comparison of the turbulence structure of subsonic and supersonic boundary layers, Phys. Fluids **1**, 1865 (1989).
[18] A. Smits and J. Dussauge, *Turbulent Shear Layers in Supersonic Flow* (Springer Science & Business Media, New York, 2006).
[19] E. Spina, A. Smits, and S. Robinson, The physics of supersonic turbulent boundary layers, Annu. Rev. Fluid Mech. **26**, 287 (1994).
[20] O. Williams, D. Sahoo, M. Baumgartner, and A. Smits, Experiments on the structure and scaling of hypersonic turbulent boundary layers, J. Fluid Mech. **834**, 237 (2018).
[21] M. Ringuette, M. Wu, and M. P. Martin, Coherent structures in direct numerical simulation of turbulent boundary layers at Mach 3, J. Fluid Mech. **594**, 59 (2008).
[22] S. Pirozzoli and M. Bernardini, Turbulence in supersonic boundary layers at moderate Reynolds number, J. Fluid Mech. **688**, 120 (2011).
[23] S. Pirozzoli, On the size of the energy-containing eddies in the outer turbulent wall layer, J. Fluid Mech. **702**, 521 (2012).
[24] M. Cogo, F. Salvadore, F. Picano, and M. Bernardini, Direct numerical simulation of supersonic and hypersonic turbulent boundary layers at moderate-high reynolds numbers and isothermal wall condition, J. Fluid Mech. **945**, A30 (2022).
[25] J. Yao and F. Hussain, Turbulence statistics and coherent structures in compressible channel flow, Phys. Rev. Fluids **5**, 084603 (2020).
[26] J. Huang, L. Duan, and M. Choudhari, Direct numerical simulation of hypersonic turbulent boundary layers: effect of spatial evolution and Reynolds number, J. Fluid Mech. **937**, A3 (2022).
[27] W. Baars, N. Hutchins, and I. Marusic, Self-similarity of wall-attached turbulence in boundary layers, J. Fluid Mech. **823**, R2 (2017).
[28] C. Cheng, W. Li, A. Lozano-Durán, and H. Liu, Uncovering townsend wall-attached eddies in low-reynolds-number wall turbulence, J. Fluid Mech. **889**, A29 (2020).
[29] C. Cheng and L. Fu, Consistency between the attached eddy model and the inner outer interaction model: a study of streamwise wall shear stress fluctuations in a turbulent channel flow, J. Fluid Mech. **942**, R9 (2022).
[30] C. Cheng, W. Shyy, and L. Fu, Streamwise inclination angle of wall-attached eddies in turbulent channel flows, J. Fluid Mech. **946**, A49 (2022).
[31] A. A. Townsend, *The Structure of Turbulent Shear Flow*, 2nd ed., (Cambridge University Press, Cambridge, England, 1976).
[32] A. E. Perry and M. S. Chong, On the mechanism of wall turbulence, J. Fluid Mech. **119**, 173 (1982).
[33] W. J. Baars and I. Marusic, Data-driven decomposition of the streamwise turbulence kinetic energy in boundary layers. Part 1. Energy spectra, J. Fluid Mech. **882**, A25 (2020).
[34] M. Yu, C. X. Xu, J. Q. Chen, P. X. Liu, Y. L. Fu, and X. X. Yuan, Spectral decomposition of wall-attached/detached eddies in compressible and incompressible turbulent channel flows, Phys. Rev. Fluids **7**, 054607 (2022).
[35] L. Fu, M. Karp, S. T. Bose, P. Moin, and J. Urzay, Shock-induced heating and transition to turbulence in a hypersonic boundary layer, J. Fluid Mech. **909**, A8 (2021).
[36] L. Fu, S. Bose, and P. Moin, Prediction of aerothermal characteristics of a generic hypersonic inlet flow, Theor. Comput. Fluid Dyn. **36**, 345 (2022).
[37] S. Gottlieb, C. Shu, and E. Tadmor, Strong stability-preserving high-order time discretization methods, SIAM Rev. **43**, 89 (2001).
[38] P. Huang, G. Coleman, and P. Bradshaw, Compressible turbulent channel flows: DNS results and modelling, J. Fluid Mech. **305**, 185 (1995).
[39] L. Agostini and M. Leschziner, On the influence of outer large-scale structures on near-wall turbulence in channel flow, Phys. Fluids **26**, 075107 (2014).
[40] L. Agostini and M. Leschziner, The connection between the spectrum of turbulent scales and the skin-friction statistics in channel flow at $Re_\tau \approx 1000$, J. Fluid Mech. **871**, 22 (2019).

[41] J. C. Del Álamo, J. Jiménez, P. Zandonade, and R. Moser, Scaling of the energy spectra of turbulent channels, J. Fluid Mech. **500**, 135 (2004).
[42] J. Jiménez, Coherent structures in wall-bounded turbulence, J. Fluid Mech. **842**, P1 (2018).
[43] R. Hirai, R. Pecnik, and S. Kawai, Effects of the semi-local Reynolds number in scaling turbulent statistics for wall heated/cooled supersonic turbulent boundary layers, Phys. Rev. Fluids **6**, 124603 (2021).
[44] A. Trettel and J. Larsson, Mean velocity scaling for compressible wall turbulence with heat transfer, Phys. Fluids **28**, 026102 (2016).
[45] A. Patel, B. J. Boersma, and R. Pecnik, The influence of near-wall density and viscosity gradients on turbulence in channel flows, J. Fluid Mech. **809**, 793 (2016).
[46] K. Griffin, L. Fu, and P. Moin, Velocity transformation for compressible wall-bounded turbulent flows with and without heat transfer, Proc. Natl. Acad. Sci. **118**, e2111144118 (2021).
[47] T. Bai, K. P. Griffin, and L. Fu, Compressible velocity transformations for various noncanonical wall-bounded turbulent flows, AIAA J. **60**, 4325 (2022).
[48] G. Elsinga, R. Adrian, B. Van Oudheusden, and F. Scarano, Three-dimensional vortex organization in a high-Reynolds-number supersonic turbulent boundary layer, J. Fluid Mech. **644**, 35 (2010).
[49] J. Monty, N. Hutchins, H. Ng, I. Marusic, and M. Chong, A comparison of turbulent pipe, channel and boundary layer flows, J. Fluid Mech. **632**, 431 (2009).
[50] J. Lee and H. Sung, Comparison of very-large-scale motions of turbulent pipe and boundary layer simulations, Phys. Fluids **25**, 045103 (2013).
[51] Y. Hwang, Statistical structure of self-sustaining attached eddies in turbulent channel flow, J. Fluid Mech. **767**, 254 (2015).
[52] C. Cheng, W. Li, A. Lozano-Durán, and H. Liu, Identity of attached eddies in turbulent channel flows with bidimensional empirical mode decomposition, J. Fluid Mech. **870**, 1037 (2019).
[53] J. Bendat and A. Piersol, *Random Data: Analysis and Measurement Procedures* (John Wiley & Sons, New York, 2011).
[54] M. Yu and C. Xu, Compressibility effects on hypersonic turbulent channel flow with cold walls, Phys. Fluids **33**, 075106 (2021).
[55] M. V. Morkovin, Effects of compressibility on turbulent flows, in *Mécanique de la Turbulence*, edited by A. Favre (CNRS, Paris, 1962), pp. 367–380.
[56] T. Cebeci, *Analysis of Turbulent Boundary Layers* (Elsevier, Amsterdam, 2012).
[57] Y. Tsuji, I. Marusic, and A. Johansson, Amplitude modulation of pressure in turbulent boundary layer, Int. J. Heat Fluid Flow **61**, 2 (2016).